Discovery of a Missing Link: First Observation of the HONO–Water Complex

Ha Vinh Lam Nguyen, Kenneth Koziol, Tarek Trabelsi, Safa Khemissi, Martin Schwell, Joseph Francisco, Isabelle Kleiner

Discovery of a Missing Link: First Observation of the HONO−Water Complex

Ha Vinh Lam Nguyen,* Kenneth J. Koziol, Tarek Trabelsi, Safa Khemissi, Martin Schwell, Joseph S. Francisco, and Isabelle Kleiner

ABSTRACT: The still unexplained daytime HONO concentration in the Earth's atmosphere and the impact of water on the HONO chemistry have been a mystery for decades. Several pathways and many modeling methods have failed to reproduce the atmospheric measurements. We reveal in this study the first spectroscopic observation and characterization of the complex of HONO with water observed through its rotational signature. Under the experimental conditions, HONO−water is stable, particularly straightforward to form, and features intense absorption signals. This could explain both the influence of water on the HONO chemistry and the missing HONO sources, as well as the missing contribution of many other molecules of atmospheric relevance that skew the accuracy of field measurements and the full account of partitioning species in the atmosphere.

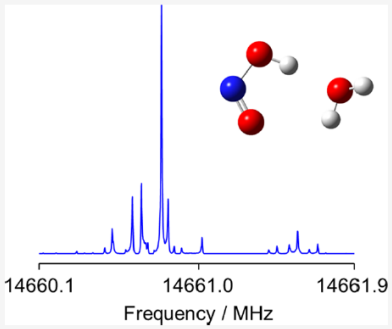

The first spectroscopic identification of HONO in 1979 showed that HONO is a photolytic active species[1] whose photochemistry provides a major source of hydroxyl radicals (OH).[2,3] The HONO concentration in air is highest at nighttime and decreases rapidly in the morning hours by decomposing, resulting in the formation of OH.[4] The contribution of HONO to the OH production is not only important in the morning but also during the day, which raises a question about the unknown HONO daytime source.[5−7] Since OH is a key species in the formation of ozone, as well as a major atmospheric oxidant causing many secondary air pollutants, a significant number of investigations on atmospheric detection and modeling have attempted to understand the genesis and decomposition of HONO.[8]

The monitoring and measuring of HONO have never been straightforward because of its high reactivity. Chemical methods such as chromatography[9] and gas and aerosol collectors[10] or spectroscopic methods such as differential optical absorption spectroscopy (DOAS),[3] long path absorption photometry (LOPAP) in the ultraviolet (UV),[11] Fourier transform infrared (FTIR) spectroscopy,[12] tunable infrared lasers[13,14] with cavity ring-down spectroscopy (CRDS),[15] and incoherent broadband cavity-enhanced absorption spectroscopy (IBBCEAS)[16] are used to determine the HONO mixing ratios. Often, a drawback of the spectroscopic measurements that rely on cross sections is the need of a clean HONO source. The lack of a pure source not only makes laboratory experiments difficult, but the HONO production is also often not completely NO_2-free since HONO exists in equilibrium with other components such as NO, NO_3, or HNO_3.

Previous studies have noted the role of relative humidity (RH) in the formation of HONO. Perner and Platt showed that the HONO concentration decreases significantly after rain, even at nighttime.[1] They suspected this observation to be due to the solubility of HONO in water. Stutz et al. reported on the nonphotolytic loss of HONO in the nocturnal atmosphere at three different locations observed by DOAS measurements for HONO and NO_2, which was explained by heterogeneous reactions or the surface adsorption of HONO by hydrolysis of NO_2.[17] The HONO/NO_2 concentration ratio did not exceed 0.04 when the RH was between 10 and 30%, but it rose to a maximum of 0.09 at higher RH. A similar study of Bernard et al. using DOAS and LOPAP measurements at nighttime showed that in 25−55% RH range, HONO formation exhibited a positive dependence on RH[18] with the highest HONO/NO_2 ratio obtained at 45−55%. At a RH > 55%, a negative dependence was observed. During daytime, the source of HONO remains unknown and cannot merely be explained by the gaseous reaction between atmospheric NO and OH. Tong et al. supposed that not only the RH but also aerosol concentrations might be important factors in the conversion of NO_2 to HONO.[19] Several mechanisms have been proposed but none of them were able to satisfactorily

Received: July 4, 2022
Accepted: August 31, 2022

explain the influence of water on the HONO chemistry in the real atmosphere. FTIR spectroscopy showed a large water effect on the HONO spectrum because water absorption underlies two HONO *Q*-branches. The impact of water in the formation of HONO was also demonstrated in experiments employing a "wet surface," which showed a dependence of HONO concentration on the water vapor in a second-order reaction.[4]

Small molecules can easily form complexes with water, for example, benzene[20] and hydroperoxy radical,[21] which leads to line shifts from the monomer. If complexes are formed, this suggests that a certain amount of the monomers will not contribute to the intensity of the monomer signals. Moreover, complexation with water influences atmospheric photolysis rates,[22] which often leads to stable reactant−water structures acting as activated states with low energy. Therefore, water complexes can serve as catalysts in atmospheric reactions.[23,24] After decades of suspecting several pathways and using many modeling methods to explain the daytime HONO concentration in the Earth atmosphere, we reveal in this study the first spectroscopic observation and characterization of the complex of HONO with water observed through its rotational signature. We suggest this to be a major missing link to explain the influence of water on the HONO chemistry and seemingly missing HONO sources.

We guided the experimental observation by performing geometry optimizations to obtain rotational constants using the standard coupled-cluster theory with single and double excitations, including a perturbative treatment of triples [CCSD(T)],[25,26] and the aug-cc-pVXZ basis sets of increasing size (X = T and Q),[27,28] as shown in Figure 1. Additionally, the

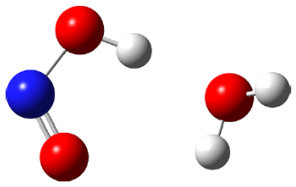

Figure 1. Structure of HONO−water calculated at the CCSD(T)/aug-cc-pVTZ level of theory.

explicitly correlated [CCSD(T)-F12] method[29,30] was also used for comparison. The dipole moments at equilibrium geometry (μ_e) are calculated in the moment of inertia principal axes system of the molecule using the finite field procedure. All of the calculations were performed in the C_1 symmetry group using the MOLPRO2019 software.[31] From the known rotational constants of *trans*- and *cis*-HONO,[32] we found that the experimental and the predicted values are very close (see Table 1). Assuming that the same is true for HONO−water, we predicted a theoretical rigid-rotor spectrum using the calculated rotational constants given in Table 1.

The laboratory production of the highly reactive HONO is a challenging issue. Several methods were developed depending on the sensitivity and the experimental characteristics of the setup in use; the basis, however, was always an acid−base reaction operated under N_2 gas with $NaNO_2$ acting as the base. In a UV and FTIR study by Barney et al., gaseous $HCl/H_2O/N_2$ was streamed over solid $NaNO_2$, which led to a large amount of HCl flowing over $NaNO_2$ without reaction and limiting the concentration of HONO to only 1.5 ppm.[33] In another study using LOPAP, HONO, also produced by the reaction between HCl and $NaNO_2$, was trapped by the azo dye unit toward the goal of obtaining very pure HONO at concentrations in the ppm order.[11]

The purity of HONO is not important when searching for the HONO−water complex using its rotational spectrum; only the concentration is required to be high enough. With the "LISA-method," a 5% H_2SO_4 solution was held in a dropping funnel and dropped at a rate of about 1 drop per 30s into a 10% solution of $NaNO_2$ (Sigma-Aldrich) under helium streamed at a backing pressure slightly higher than atmospheric pressure. The product mixture is expanded directly into the Fabry−Pérot type resonator vacuum chamber through a pulsed nozzle. The spectrum was recorded using two molecular jet FT microwave spectrometers operating from 2 to 40 GHz.[34,35] All signals appearing in the survey spectrum with a grid of 250 kHz were later remeasured at a higher resolution with an experimental accuracy of 2 kHz, where they appear as doublets because of the Doppler effect arising from the coaxial arrangement of the resonator and the molecular jet. The intense $4_{04} \leftarrow 3_{13}$ rotational transitions, located at 17 266.3 MHz for *trans*-HONO (see Figure 2) and at 31 221.9 for *cis*-HONO, were used as references to ensure the HONO concentration to be sufficient. Mean velocity calculations from the Doppler splitting observed in measurements at high resolution (2 kHz) due to the coaxial arrangement between the resonator and the molecular jet indicate that the gas mixture contains at least 5% HONO.

The HONO−water rotational spectrum is dominated by *a*-type transitions. Therefore, we first searched for three rotational transitions of the same *a*-type *R*-branch $2_{02} \leftarrow 1_{01}$, $2_{12} \leftarrow 1_{11}$, and $2_{11} \leftarrow 1_{10}$ and found them red-shifted from the predicted frequencies by almost the same difference, which was the key for the success in spectral assignment (see Table 2). Fitting these three transitions allowed for an improved spectral

Table 1. Calculated (calc.) and Observed (obs.) Rotational Constants (in MHz) of *trans* and *cis*-HONO and HONO−Water, as Well as the Calculated Dipole Moment Components (in Debye)[a]

	trans-HONO		*cis*-HONO		HONO−water	
	calc.	obs.	calc.	obs.	calc.	obs.
A	92451.0	92889.1	83417.1	84101.7	13095.2	12449.6(11)
B	12554.5	12524.8	13205.4	13169.0	4342.1	4226.499(27)
C	11053.4	11016.8	11400.6	11364.3	3276.7	3152.990(18)
μ_a	1.64		0.45		2.95	
μ_b	1.55		1.32		0.91	
μ_c	0.00		0.00		1.26	

[a]Calculations are performed at the CCSD(T)/aug-cc-pVTZ level of theory.

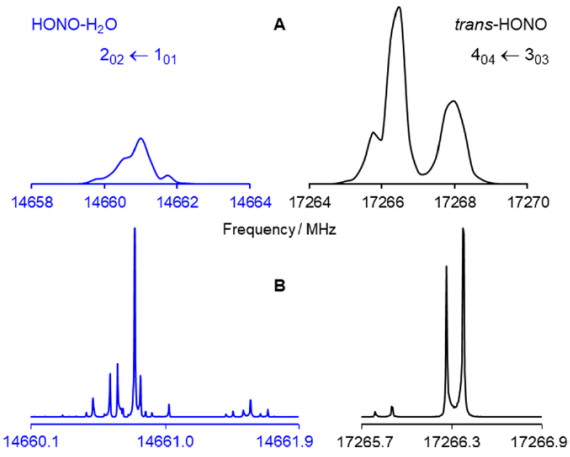

Figure 2. (A) Two sections of the broadband scan illustrating the $4_{04} \leftarrow 3_{13}$ rotational transition of *trans*-HONO (right-hand side) and the $2_{02} \leftarrow 1_{01}$ transition of HONO–water (left-hand side). The absolute intensities are scaled. The measurement grid is 250 kHz. (B) The same transitions recorded at high resolution (2 kHz). Intensities are normalized. For both (A) and (B) figures, the frequency axes are scaled for a reasonable comparison.

Table 2. Calculated (calc.) and Observed (obs.) Frequencies (in MHz) of Some HONO–Water Transitions Labeled by the Rotational Quantum Numbers[a]

$J''_{K''_a K''_c} \leftarrow J'_{K'_a K'_c}$	calc.	obs.	obs.–calc.
$1_{01} \leftarrow 0_{00}$	7618.8	7379.5	−239
$2_{02} \leftarrow 1_{01}$	15146.2	14660.4	−486
$2_{12} \leftarrow 1_{11}$	14172.2	13685.2	−487
$2_{11} \leftarrow 1_{10}$	16303.1	15832.5	−471

[a]The complete list is given in the Supporting Information.

prediction that resulted in the detection of 24 other transitions measurable in the operating frequency range of the two spectrometers and secured that the detected signals belonged to HONO–water. Some weak *b*-type transitions could also be measured and increased the accuracy of the determined *A* rotational constant.

A typical spectrum of the $2_{02} \leftarrow 1_{01}$ transition captured in the broadband survey, as well as recorded at high resolution, is illustrated in Figure 2. The high-resolution spectra of HONO–water show much more complex hyperfine structures than those obtained for the HONO monomer (see, for example, the lower trace of Figure 2). While those of the HONO monomer feature typical patterns of ^{14}N nuclear quadrupole coupling, the spectra of HONO–water are governed by many additional small splittings of up to 200 kHz. At the beginning, we suspected these splittings to arise from the large amplitude tunneling motions (LAMs) of water with two possible cases. (1) Since the equilibrium structure predicted an out-of-plane hydrogen atom in the water moiety, as visualized in Figure 1, there is a chance of the water making a ring-puckering-like motion where this hydrogen atom tunnels through the heavy-atom plane to an equivalent structure on the opposite side (tunneling between configurations II and III in the potential energy curve given in Figure 3). If present, split *c*-type transitions with the interstate selection rule (+) ↔ (−) would be observed, and the splittings might be large due to the small

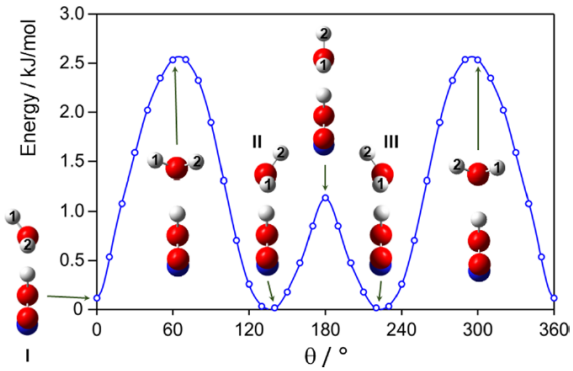

Figure 3. Potential energy curve of HONO–water obtained by rotating the water molecule around its C_{2v} axis. LAM (1) (see text) corresponds to the tunneling between configurations II and III through a hindering barrier of only 1.2 kJ/mol. LAM (2) (hydrogen permutation) is the tunneling between configurations I and II or I and III with a slightly higher barrier of 2.5 kJ/mol. Both LAMs are most probably feasible.

weight of the hydrogen atom compared with that of the frame.[36] This is strongly supported by the nonobservation of any *c*-type line despite the μ_c dipole moment component of 1.26 D being comparable with μ_b = 0.91 D (see Table 1) while *b*-type transitions are observed. However, this motion would still split all *a*-type transitions to doublets with the intrastate selection rules (+) ↔ (+) and (−) ↔ (−) because of Coriolis interactions, and the intensity of the doublet components should be the same. (2) The second possibility is the case of water rotating on its C_{2v} axis, where the two hydrogen atoms permute (tunneling between configurations I and II or I and III in Figure 3). In this case, there would be doublet splitting of all the observed transitions, but no transitions cross states. Therefore, the splitting is likely small and fits the 200 kHz order of magnitude. The expected ratio of the doublet components would be 3:1 due to the ortho/para ratio of the hydrogen atoms and should hold for all transitions.

After many assignment and fitting attempts and from the repeated appearance of a triplet structure, as shown exemplarily in Figure 4, we turned to thinking that the very complex splitting patterns are not caused by the two LAMs, but by the spin–spin coupling of the two hydrogen atoms in the water molecule and, to some extent, also with the hydrogen atom of HONO. However, from a few available investigations in the literature[37,38] and a test prediction, splitting due to this coupling should be less than 20 kHz. Thus, we finally returned to the initial explanation that the splitting is caused by a combination of the two tunneling motions of water, which cannot be described by a combination of a doublet with similar intensity and a doublet with 3:1 intensity ratio. Exhaustive group theoretical treatment of HONO–water is required to help the spectral assignment, as has been done for the water dimer complex.[39] At presence, a fit considering only the nuclear quadrupole hyperfine splittings of the ^{14}N nucleus is given in the Supporting Information, and the rotational constants are compared with the theoretical values in Table 1, which show a high consistency. The fitted frequencies and obtained molecular parameters are available in the Supporting Information along with the observed-minus-calculated values.

The Doppler splittings of HONO–water lines that are smaller than the square root of their inverse mass ratio indicate

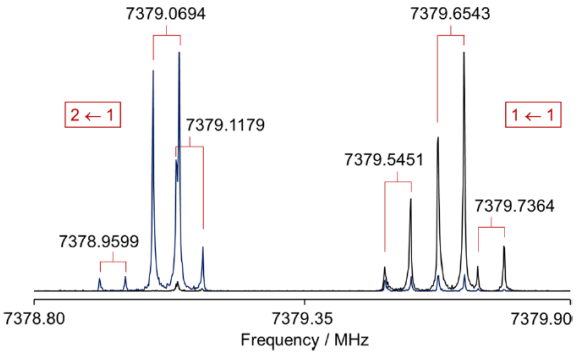

Figure 4. Two high resolution spectra of the $1_{01} \leftarrow 0_{00}$ rotational transition of HONO–water indicating further splittings on top of the $F' \leftarrow F$: 2 ← 1 and 1 ← 1 nuclear quadrupole coupling components. The polarization frequencies are 7378.9 and 7379.8 MHz for the dark blue and black spectra, respectively. Doppler doublets are marked by brackets. Intensities are normalized.

that the gas mixture contains more HONO–water (about 7%) than HONO, which hints that the complexation of HONO with water is particularly straightforward. The line shift caused by this complexation is remarkable. Taking the $2_{02} \leftarrow 1_{01}$ transition as an example, the *trans*-HONO line at 47 061.8 MHz[32] is red-shifted to 14 660.4 MHz in the HONO–water complex. The shift is even more significant higher in the energy ladder. For example, a red shift of about 30 cm^{-1} has been observed for acetylene–water complex in the IR range.

HONO–water does not only just exist. It is also relatively stable and easy to form under our experimental conditions. If the missing daytime HONO source is its complexation, this situation could also explain the missing spectral presence of many other molecules of atmospheric relevance that skew the accuracy of field measurements and the full account of partitioning species in the atmosphere.

■ ASSOCIATED CONTENT

Supporting Information

The Supporting Information is available free of charge at https://pubs.acs.org/doi/10.1021/acs.jpclett.2c02081.

Calculated rotational constants of *trans*- and *cis*-HONO and HONO–water and their nuclear coordinates, fitted frequencies of HONO–water, and fitted molecular parameters of HONO–water (PDF)

■ AUTHOR INFORMATION

Corresponding Author

Ha Vinh Lam Nguyen – *Univ Paris Est Creteil and Université Paris Cité, CNRS, LISA, F-94010 Créteil, France; Institut Universitaire de France (IUF), F-75231 Paris Cedex 05, France;* orcid.org/0000-0002-5493-8905; Email: lam.nguyen@lisa.ipsl.fr

Authors

Kenneth J. Koziol – *Institute of Physical Chemistry, RWTH Aachen University, D-52074 Aachen, Germany*

Tarek Trabelsi – *Department of Earth and Atmospheric Science and Department of Chemistry, University of Pennsylvania, Philadelphia, Pennsylvania 19104, United States;* orcid.org/0000-0001-6258-7191

Safa Khemissi – *Univ Paris Est Creteil and Université Paris Cité, CNRS, LISA, F-94010 Créteil, France*

Martin Schwell – *Univ Paris Est Creteil and Université Paris Cité, CNRS, LISA, F-94010 Créteil, France*

Joseph S. Francisco – *Department of Earth and Atmospheric Science and Department of Chemistry, University of Pennsylvania, Philadelphia, Pennsylvania 19104, United States;* orcid.org/0000-0002-5461-1486

Isabelle Kleiner – *Université Paris Cité and Univ Paris Est Creteil, CNRS, LISA, F-75013 Paris, France*

Complete contact information is available at: https://pubs.acs.org/10.1021/acs.jpclett.2c02081

Notes

The authors declare no competing financial interest.

The high-resolution spectra with a complete list of observed transitions are available with H.V.L.N.

■ ACKNOWLEDGMENTS

We thank Dr. J. Kleffmann (Wuppertal University) and Prof. Dr. J.-F. Doussin (laboratory LISA) for discussions on the HONO production, as well as Prof. Dr. D. A. Obenchain for exchanges and discussions on the spectral analysis. This work was supported by the French National program LEFE (Les Enveloppes Fluides et l'Environnement) and the Agence Nationale de la Recherche ANR (project ID ANR-18-CE29-0011).

■ REFERENCES

(1) Perner, D.; Platt, U. Detection of Nitrous Acid in the Atmosphere by Differential Optical Absorption. *Geophys. Res. Lett.* **1979**, *6*, 917–920.

(2) Saliba, N. A.; Mochida, M.; Finlayson-Pitts, B. J. Laboratory Studies of Sources of HONO in Polluted Urban Atmospheres. *Geophys. Res. Lett.* **2000**, *27*, 3229–3232.

(3) Wennberg, P. O.; Dabdub, D. Rethinking Ozone Production. *Science* **2008**, *319*, 1624–1625.

(4) Lammel, G.; Cape, J. N. Nitrous Acid and Nitrite in the Atmosphere. *Chem. Soc. Rev.* **1996**, *25*, 361–369.

(5) Acker, K.; Möller, D.; Wieprecht, W.; Meixner, F. X.; Bohn, B.; Gilge, S.; Plass-Dülmer, C.; Berresheim, H. Strong Daytime Production of OH from HNO_2 at a Rural Mountain Site. *Geophys. Res. Lett.* **2006**, *33*, L02809.

(6) Kleffmann, J. Daytime Sources of Nitrous Acid (HONO) in the Atmospheric Boundary Layer. *ChemPhysChem* **2007**, *8*, 1137–1144.

(7) Michoud, V.; Colomb, A.; Borbon, A.; Miet, K.; Beekmann, M.; Camredon, M.; Aumont, B.; Perrier, S.; Zapf, P.; Siour, G.; Ait-Helal, W.; Afif, C.; Kukui, A.; Furger, M.; Dupont, J. C.; Haeffelin, M.; Doussin, J. F. Study of the Unknown HONO Daytime Source at a European Suburban Site during the MEGAPOLI Summer and Winter Field Campaigns. *Atmos. Chem. Phys.* **2014**, *14*, 2805–2822.

(8) Aumont, B.; Chervier, F.; Laval, S. Contribution of HONO Sources to the $NO_x/HO_x/O_3$ Chemistry in the Polluted Boundary Layer. *Atmos. Environ.* **2003**, *37*, 487–498.

(9) Xue, C.; Ye, C.; Ma, Z.; Liu, P.; Zhang, Y.; Zhang, C.; Tang, K.; Zhang, W.; Zhao, X.; Wang, Y.; Song, M.; Liu, J.; Duan, J.; Qin, M.; Tong, S.; Ge, M.; Mu, Y. Development of Stripping Coilion Chromatograph Method and Intercomparison with CEAS and LOPAP to Measure Atmospheric HONO. *Sci. Total Environ.* **2019**, *646*, 187–195.

(10) Dong, H.-B.; Zeng, L.-M.; Hu, M.; Wu, Y.-S.; Zhang, Y.-H.; Slanina, J.; Zheng, M.; Wang, Z.-F.; Jansen, R. The Application of an Improved Gas and Aerosol Collector for Ambient Air Pollutants in China. *Atmos. Chem. Phys.* **2012**, *12*, 10519–10533.

(11) Heland, J.; Kleffmann, J.; Kurtenbach, R.; Wiesen, P. A New Instrument to Measure Gaseous Nitrous Acid (HONO) in the Atmosphere. *Environ. Sci. Technol.* **2001**, *35*, 3207−3212.
(12) Stockwell, C. E.; Yokelson, R. J.; Kreidenweis, S. M.; Robinson, A. L.; DeMott, P. J.; Sullivan, R. C.; Reardon, J.; Ryan, K. C.; Griffith, D. W. T.; Stevens, L. Trace Gas Emissions from Combustion of Peat, Crop Residue, Domestic Biofuels, Grasses, and Other Fuels: Configuration and Fourier Transform Infrared (FTIR) Component of the Fourth Fire Lab at Missoula Experiment (FLAME-4). *Atmos. Chem. Phys.* **2014**, *14*, 9727−9754.
(13) Lee, B. H.; Wood, E. C.; Zahniser, M. S.; McManus, J. B.; Nelson, D. D.; Herndon, S. C.; Santoni, G. W.; Wofsy, S. C.; Munger, J. W. Simultaneous Measurements of Atmospheric HONO and NO_2 via Absorption Spectroscopy Using Tunable Mid-Infrared Continuous-Wave Quantum Cascade Lasers. *Appl. Phys. B: Laser Opt.* **2011**, *102*, 417−423.
(14) Schiller, C. L.; Locquiao, S.; Johnson, T. J.; Harris, G. W. Atmospheric Measurements of HONO by Tunable Diode Laser Absorption Spectroscopy. *J. Atmos. Chem.* **2001**, *40*, 275−293.
(15) Wang, L. M.; Zhang, J. S. Detection of Nitrous Acid by Cavity Ring Down Spectroscopy. *Environ. Sci. Technol.* **2000**, *34*, 4221−4227.
(16) Tang, K.; Qin, M.; Fang, W.; Duan, J.; Meng, F.; Ye, K.; Zhang, H.; Xie, P.; He, Y.; Xu, W.; Liu, J.; Liu, W. Simultaneous Detection of Atmospheric HONO and NO_2 Utilising an IBBCEAS System Based on an Iterative Algorithm. *Atmos. Meas. Technol.* **2020**, *13*, 6487−6499.
(17) Stutz, J.; Alicke, B.; Ackermann, R.; Geyer, A.; Wang, S.; White, A. B.; Williams, E. J.; Spicer, C. W.; Fast, J. D. Relative Humidity Dependence of HONO Chemistry in Urban Areas. *J. Geophys. Res.* **2004**, *109*, D03307.
(18) Bernard, F.; Cazaunau, M.; Grosselin, B.; Zhou, B.; Zheng, J.; Liang, P.; Zhang, Y.; Ye, X.; Daële, V.; Mu, Y.; Zhang, R.; Chen, J.; Mellouki, A. Measurements of Nitrous Acid (HONO) in Urban Area of Shanghai, China. *Environ. Sci. Pollut. Res.* **2016**, *23*, 5818−5829.
(19) Tong, S.; Hou, S.; Zhang, Y.; Chu, B.; Liu, Y.; He, H.; Zhao, P.; Ge, M. Exploring the Nitrous Acid (HONO) Formation Mechanism in Winter Beijing: Direct Emissions and Heterogeneous Production in Urban and Suburban Areas. *Faraday Discuss.* **2016**, *189*, 213−230.
(20) Gruenloh, C. J.; Carney, J. R.; Arrington, C. A.; Zwier, T. S.; Fredericks, S. Y.; Jordan, K. D. Infrared Spectrum of a Molecular Ice Cube: The S_4 and D_{2d} Water Octamers in Benzene-$(Water)_8$. *Science* **1997**, *276*, 1678−1681.
(21) Suma, K.; Sumiyoshi, Y.; Endo, Y. The Rotational Spectrum of the Water-Hydroperoxy Radical (H_2O-HO_2) Complex. *Science* **2006**, *311*, 1278−1281.
(22) Vaida, V. Perspective: Water Cluster Mediated Atmospheric Chemistry. *J. Chem. Phys.* **2011**, *135*, 020901.
(23) Li, H.; Zhong, J.; Vehkamäki, H.; Kurtén, T.; Wang, W.; Ge, M.; Zhang, S.; Li, Z.; Zhang, X.; Francisco, J. S.; Zeng, X. C. Self-Catalytic Reaction of SO_3 and NH_3 to Produce Sulfamic Acid and its Implication to Atmospheric Particle Formation. *J. Am. Chem. Soc.* **2018**, *140*, 11020−11028.
(24) Hansen, J. C.; Francisco, J. S. Radical-Molecule Complexes: Changing our Perspective on the Molecular Mechanisms of Radical-Molecule Reactions and their Impact on Atmospheric Chemistry. *ChemPhysChem* **2002**, *3*, 833−840.
(25) Knowles, P. J.; Hampel, C.; Werner, H.-J. Coupled Cluster Theory for High Spin, Open Shell Reference Wave Functions. *J. Chem. Phys.* **1993**, *99*, 5219.
(26) Knowles, P. J.; Hampel, C.; Werner, H.-J. Erratum: "Coupled Cluster Theory for High Spin, Open Shell Reference Wave Functions. *J. Chem. Phys.* **2000**, *112*, 3106.
(27) Dunning, T. H. Gaussian Basis Sets for Use in Correlated Molecular Calculations. I. The Atoms Boron through Neon and Hydrogen. *J. Chem. Phys.* **1989**, *90*, 1007.
(28) Dunning, T. H.; Peterson, K. A.; Wilson, A. K. Gaussian Basis Sets for Use in Correlated Molecular Calculations. X. The Atoms Aluminum through Argon Revisited. *J. Chem. Phys.* **2001**, *114*, 9244.
(29) Adler, T. B.; Knizia, G.; Werner, H.-J. A Simple and Efficient CCSD(T)-F12 Approximation. *J. Chem. Phys.* **2007**, *127*, 221106.
(30) Knizia, G.; Adler, T. B.; Werner, H.-J. Simplified CCSD(T)-F12 Methods: Theory and Benchmarks. *J. Chem. Phys.* **2009**, *130*, 054104.
(31) Werner, H.-J.; Knowles, P. J.; Knizia, G.; Manby, F. R.; Schütz, M.; Celani, P.; Györffy, W.; Kats, D.; Korona, T.; Lindh, R.; Mitrushenkov, A.; Rauhut, G.; Shamasundar, K. R.; Adler, T. B.; Amos, R. D.; Bennie, S. J.; Bernhardsson, A.; Berning, A.; Cooper, D. L.; Deegan, M. J. O.; Dobbyn, A. J.; Eckert, F.; Goll, E.; Hampel, C.; Hesselmann, A.; Hetzer, G.; Hrenar, T.; Jansen, G.; Köppl, C.; Lee, S. J. R.; Liu, Y.; Lloyd, A. W.; Ma, Q.; Mata, R. A.; May, A. J.; McNicholas, S. J.; Meyer, W.; T. F., Miller, III; Mura, M. E.; Nicklass, A.; O'Neill, D. P.; Palmieri, P.; Peng, D.; Pflüger, K.; Pitzer, R.; Reiher, M.; Shiozaki, T.; Stoll, H.; Stone, A. J.; Tarroni, R.; Thorsteinsson, T.; Wang, M.; Welborn, M. *MOLPRO, version 2019.1, a package of ab initio programs*; Molpro, 2019.
(32) Cox, A. P.; Brittain, A. H.; Finnigan, D. J. Microwave Spectrum, Structure, Dipole Moment and Quadrupole Coupling Constants of *Cis* and *Trans* Nitrous Acids. *Trans. Faraday Soc.* **1971**, *67*, 2179−2194.
(33) Barney, W. S.; Wingen, L. M.; Lakin, M. J.; Brauers, T.; Stutz, J.; Finlayson-Pitts, B. J. Infrared Absorption Cross-Section Measurements for Nitrous Acid (HONO) at Room Temperature. *J. Phys. Chem. A* **2000**, *104*, 1692−1699.
(34) Grabow, J.-U.; Stahl, W.; Dreizler, H. A Multioctave Coaxially Oriented Beam-Resonator Arrangement Fourier-Transform Microwave Spectrometer. *Rev. Sci. Instrum.* **1996**, *67*, 4072−4084.
(35) Merke, I.; Stahl, W.; Dreizler, H. A Molecular Beam Fourier Transform Microwave Spectrometer in the Range 26.5 to 40 GHz. Tests of Performance and Analysis of the D- and ^{14}N-Hyperfine Structure of Methylcyanide-d_1. *Z. Naturforsch. A* **1994**, *49*, 490−496.
(36) Nguyen, H. V. L.; Gulaczyk, I.; Kręglewski, M.; Kleiner, I. Large Amplitude Inversion Tunneling Motion in Ammonia, Methylamine, Hydrazine, and Secondary Amines: From Structure Determination to Coordination Chemistry. *Coord. Chem. Rev.* **2021**, *436*, 213797.
(37) Jahn, M. K.; Obenchain, D. A.; Nair, K. P. R.; Grabow, J.-U.; Vogt, N.; Demaison, J.; Godfrey, P. D.; McNaughton, D. The Puzzling Hyper-Fine Structure and an Accurate Equilibrium Geometry of Succinic Anhydride. *Phys. Chem. Chem. Phys.* **2020**, *22*, 5170−5177.
(38) Grubbs, G. S., II; Obenchain, D. A.; Pickett, H. M.; Novick, S. E. H2—AgCl: A Spectroscopic Study of a Dihydrogen Complex. *J. Chem. Phys.* **2014**, *141*, 114306.
(39) Coudert, L. H.; Hougen, J. T. Tunneling Splittings in the Water Dimer: Further Development of the Theory. *J. Mol. Spectrosc.* **1988**, *130*, 86−119.